INTERNATIONAL JOURNAL OF HYDROGEN ENERGY 33 (2008) 2273–2282

Available at www.sciencedirect.com

ScienceDirect

journal homepage: www.elsevier.com/locate/he

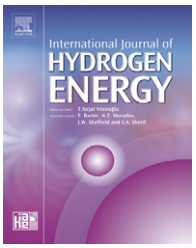

Dynamic modeling and analysis of a shell-and-tube type gas-to-gas membrane humidifier for PEM fuel cell applications

Sang-Kyun Park[a], *Song-Yul Choe*[a,*], *Seo-ho Choi*[b]

[a]*Mechanical Engineering Department, Auburn University, Auburn, AL 36848, USA*
[b]*Fuel Cell Vehicle Team, Hyundai Motor Company and Kia Motors Corporation, Korea*

ARTICLE INFO

Article history:
Received 6 February 2007
Received in revised form
27 December 2007
Accepted 23 February 2008
Available online 10 April 2008

Keywords:
PEMFC
Gas-to-gas membrane humidifier
Shell- and- tube
Mass transfer
Heat transfer

ABSTRACT

A gas-to-gas humidifier using membranes is the preferred technology for external humidification of fuel cell reactant gases in mobile applications because no extra power supply is required and there are no moving parts. In particular, a shell and tube structure is compact, which allows its easier integration in a fuel cell vehicle.

This paper proposes a mathematical model for the humidifier using the principles of thermodynamics, including analysis of heat and mass transfer and of static and dynamic behaviors. Firstly, the heat and mass transfer behavior was simulated and the results compared with the experimental data. Secondly, the model was used to investigate the sensitivity of the geometric parameters and the effects of various operating conditions on performance. Finally, step responses of the humidifier at various flow rates were analyzed.

1. Introduction

Proper management of water in an operating polymer electrolyte membrane (PEM) fuel cell stack is one of the most important factors to prevent performance degradation and improve cell reliability. Improper humidification may on one hand increase the ohmic voltage losses, and on the other hand cause flooding in the cathode side clogging the pathway of the reactants.

The membrane is an ionomer that blocks migration of electrons and at the same time allows for transport of protons generated by hydrogen oxidation on the anode side. The protons crossing the membrane take up water molecules. Thus, a gradient of water concentration from the anode to the cathode side is formed [1,2]. In contrast, a low gradient of water concentration on the anode side causes a back diffusion from the cathode side where water is produced by oxygen reduction. Thus, appropriate water balance in the membranes is necessary to allow high mobility of protons, which ultimately reduces ohmic over-potentials. On the other hand, the membranes can be dehydrated under operating conditions when the working temperature rises above 60 °C. Here, the air supplied dries out the electrodes quicker than water can be produced by the reaction. In this case, extra humidification is needed to prevent dehydration of the membranes [3].

Flooding is the second concern and can occur on the cathode side when high currents are applied. When the water produced in the catalyst is not removed properly, the water residing in the pores of the gas diffusion layer (GDL) blocks the pathway of the reactants. The lack of the reactants reduces the chemical reaction rates and increases the over-potential [4]. Therefore, different technologies are employed to maintain water balance in a stack. In regard to maintaining

*Corresponding author. Tel.: +1 344 844 3328.
E-mail address: choe@eng.auburn.edu (S.-Y. Choe).
0360-3199/$ - see front matter
doi:10.1016/j.ijhydene.2008.02.058

Nomenclature

A	humidifier membrane area, cm^2
a	water activity
C	water concentration, $mol\,cm^{-3}$
C_p	specific heat of constant pressure, $J\,kg^{-1}\,K^{-1}$
C_v	specific heat of constant volume, $J\,kg^{-1}\,K^{-1}$
D_i	hydraulic diameter, m
D_w	membrane diffusion coefficient, $cm^2\,s^{-1}$
h	enthalpy, J
h_i	heat transfer coefficient
k	gas thermal conductivity, $W\,m^{-1}\,K^{-1}$
M	molecular mass, $kg\,mol^{-1}$
$M_{mem,dry}$	membrane dry equivalent weight, $kg\,mol^{-1}$
m	mass, kg
Nu	Nusselt number
P	pressure, Pa
Pr	Prandtl number
R	gas constant, $J\,kg^{-1}\,K^{-1}$
Re	Reynolds number
RH	relative humidity
T	temperature, K
t_{mem}	membrane thickness, cm
Q	heat, J
U	overall heat transfer coefficient, $W\,m^{-2}\,K^{-1}$
u	internal energy, J
V	volume, m^3
x	constant

Greek symbols

ρ	density, $kg\,cm^{-3}$
λ	water content
ω	humidity ratio
ΔT_{lm}	logarithmic mean temperature difference, K

Superscripts and subscripts

1	control volume 1
2	control volume 2
g	gas
i	tube side or shell side
in	inlet
$k1$	control volume 1 or 2
$k2$	gas or vapor
$k3$	inlet, outlet or transfer
mem	membrane
out	outlet
v	vapor
y	constant

the water balance a stack design may employ porous bipolar plates [5] allowing for water transfer. In another design, two micro-layers with a different mixing ratio between electron conducting and hydrophobic materials for the GDL were proposed to perform a high rate of water removal [6]. However, none of the technologies has completely resolved the concerns about water balance in an operating stack that still plays a key role in ensuring performance and reliability.

The humidity in a stack can be manipulated by changing the operating conditions of inlets and outlets at both the anode and cathode side, relationships that were intensively investigated [7,8]. The external humidifiers currently used are nozzle spray, gas bubbling, enthalpy wheel and membrane humidifiers [9–11]. The humidifiers employing nozzle spray and gas bubbling require an extra heater to elevate the temperature of water, which results in an increase in the weight, complexity, parasitic power losses and high costs. Conversely, the enthalpy wheel and the membrane humidifier have proven to be more viable techniques for mobile applications than others because they reuse the large amount of the heat and moisture carried by the exhaust gas from the outlet of the cathode side, where the heat is used for preheating the inlet air and the moisture is recaptured. As a result, the overall efficiency of the fuel cell system is improved.

The enthalpy wheel humidifier requires a rotating part driven by an electric motor that requires additional electric power. Humidifiers using membranes do not need any moving parts and allow for more energy efficient operation. Thus, the membrane type humidifier is preferred in vehicle applications.

Design of the gas-to-gas humidifier with membranes employs two different shapes, a rectangular cubical and a cylindrical form. The membranes serve as a separator that prevents two different fluid flows from mixing. At the same time, the membrane allows for the exchange of heat and water between the two fluid flows. Therefore, the performance of a humidifier is dependent upon the geometric dimensions of the membranes along with their properties, the state of the fluids and the shape of flow channels.

On the other hand, heat and mass transfer in the membrane determine the performance of humidification. The mechanism of the humidifier and design parameters were investigated by Zhang et al. [12] using a mathematical model for a humidity pump with a counter flow. The performance of the pump was inversely proportional to the membrane thickness and was increased by a large temperature difference between two inlets. Daud [13] proposed a cross-flow design that included the effect of a trans-membrane pressure drop and concentration polarization along the tube for a tubular membrane module. However, dynamic aspects were not fully considered. In fact, the dynamic heat and mass transfer characteristics of the membranes necessary for design of a humidifier were studied by Chen and Peng [14], but the shape was cubical. Therefore, our study focused on a shell-and-tube type gas-to-gas membrane humidifier, where the heat and mass transfer behavior was analyzed under different operating conditions. Also included are parametric studies of geometric factors on the performance of the humidifier and the dynamic characteristics. The model was implemented using block sets given in MATLAB/SIMULINK and simulations were performed.

2. Physical structure and operating principle

The humidifier examined was a shell-and-tube type gas-to-gas membrane humidifier that consists of a bundle of membrane tubes arranged as a shell and tube heat exchanger shown in Fig. 1. When dry inlet air flows through the inside of the bundle tubes, the air is humidified and at the same time absorbs heat from the fuel cell stack exhaust air that flows around the outside of the tubes and transfers heat and moisture being carried to those of the dry inlet gas. Depending upon the layout of flow directions of the inlet and the exhaust gas, two designs are possible, a parallel or a counter flow. The parallel flow design allows the dry and exhaust air to flow in the same direction, while the counter flow design allows them to flow in opposite directions.

In principle, the humidifier can be explained by applying heat and mass transfer in two control volumes. In fact, the heat transfer behavior of a membrane is comparable with that of a heat exchanger, while the mass transfer of the vapor in the membrane is directly related to the water content and diffusivity in the membrane that are affected by the water activity and temperature at both sides of the membrane.

Fig. 2 shows a simplified humidifier with a counter flow. The setup is divided into two control volumes; one for the dry air (control volume 1, tube side) and one for the stack exhaust air side (control volume 2, shell side). For a parallel flow, the position of the inlet and the exhaust is switched, but the two control volumes remain as before. Inlet conditions for each of two control volumes are inlet mass flow, M_{in}, temperature, T_{in}, pressure, P_{in} and relative humidity, RH_{in}, while outlet conditions are gas outlet mass flow, M_{out}, temperature, T_{out}, pressure, P_{out} and relative humidity, RH_{out}. The parameters of the shell-and-tube type gas-to-gas membrane humidifier are listed in Table 1.

Hence, the humidifier is described mathematically using the following assumptions:

(a) all gases are ideal gases;
(b) there are negligible kinetic and potential energy changes;

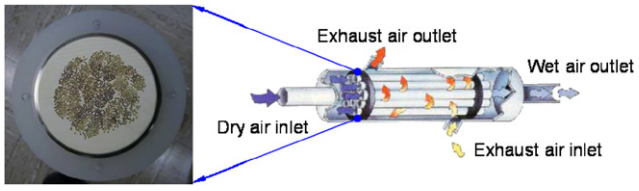

Fig. 1 – Structure of a shell-and-tube type gas-to-gas membrane humidifier [15].

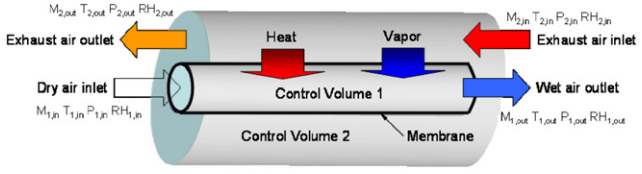

Fig. 2 – Simplified setup for modeling of a humidifier.

Table 1 – Humidifier parameters for a Perma Pure FC 200-780-10PP

Parameters	Value
Thickness of the membrane tube	0.00005 m
Inner diameter of the membrane tube	0.00097 m
Active length of the membrane tube	0.254 m
Overall length of the membrane tube	0.311 m
Number of the membrane tubes	780
Inner diameter of the humidifier housing	0.056 m
Membrane dry density	0.001 kg cm^{-3}
Membrane dry equivalent weight	1.0 kg mol^{-1}

(c) because of perfect insulation, there are no heat losses and only the heat transfer across the membrane occurs;
(d) the specific heat coefficients are constant;
(e) no liquid phase species and condensation within the humidifier is considered;
(f) the diameters of the individual control volume are equal to the inner diameter;
(g) the tube consists of a single membrane, where the diameter and area are equal to the sum of the diameters and areas of all tubes.

In addition, the high humidity and elevated temperature of the exhaust gas from the stack allowed for the assumption that heat and vapor present in control volume 2 were mainly transferred to control volume 1.

3. Modeling approach

Using the two control volumes, we developed a model for a shell-tube type humidifier by applying the principles of thermodynamics—mass and heat transfer.

3.1. *Thermodynamics*

The heat in the control volume is equal to the sum of the heat flowing in, flowing out and the variation of the internal energy in the control volume. Accordingly, a thermal dynamic behavior of air in a shell and a tube side was governed by the following equations [14,16];

$$\sum \frac{dm_{k1,k2,out}}{dt} \cdot h_{k1,k2,out} = \frac{dQ_{k1}}{dt} + \sum \frac{dm_{k1,k2,in}}{dt} \cdot h_{k1,k2,in} + \frac{dm_{k1,v,trans}}{dt} \cdot h_{trans} - \left(\frac{dm_{k1,k2}}{dt} \cdot u_{k1,k2} + \frac{du_{k1,k2}}{dt} \cdot m_{k1,k2} \right). \quad (1)$$

Hence, the internal energy and the enthalpy are equal to the product of the temperature variation and the specific heat.

$$\frac{du_{k1,k2}}{dt} = C_{v,k2} \cdot \frac{dT_{k1}}{dt}, \frac{dh_{k1,k2,k3}}{dt} = C_{p,k2} \cdot \frac{dT_{k1,k3}}{dt}. \quad (2)$$

In addition, the variation of the mass in the control volumes was obtained by applying the mass conservation

equation (Eq. (3)) and the ideal gas law (Eq. (4)), where the relative humidity was defined as a ratio of the vapor and the saturated vapor pressure (Eq. (5)).

$$\frac{dm_{k1,k2}}{dt} = \sum \frac{m_{k1,k2,in}}{dt} - \sum \frac{m_{k1,k2,out}}{dt}, \tag{3}$$

$$P_{k1,k2,out} \cdot V_{k1} = R_{k2} \cdot T_{k1,out} \cdot m_{k1,k2}, \tag{4}$$

$$\omega_{1,k3} = \frac{M_v \cdot P_{1,v,k3}}{M_g \cdot P_{1,g,k3}}, \omega_{2,k3} = \frac{M_v \cdot P_{2,v,k3}}{M_g \cdot P_{2,ex,k3}}, RH_{k1,k3} = \frac{P_{k1,v,k3}}{P_{k1,sat,k3}}. \tag{5}$$

Then, the outlet mass flow rate was defined as follows:

$$\frac{dm_{1,g,k3}}{dt} = \frac{1}{1+\omega_{1,k3}} \frac{dm_{1,k3}}{dt}, \frac{dm_{2,g,k3}}{dt} = \frac{1}{1+\omega_{2,k3}} \frac{dm_{2,k3}}{dt}. \tag{6}$$

3.2. Heat transfer

The heat transfer behavior is governed by the energy equation, where the coefficients are obtained for the tubular geometry. The heat transfer rate across the membrane is given as follows [17]:

$$\frac{dQ_{k1}}{dt} = U \cdot A \cdot \Delta T_{lm}, \tag{7}$$

where U is the overall heat transfer coefficient ($W\,m^{-2}\,K^{-1}$) that is a function of the convective heat transfer coefficients of the air, h.

$$\frac{1}{U \cdot A} = \frac{1}{h_{tubeside} \cdot A_{inner}} + \frac{\ln(D_{outer}/D_{inner})}{2\pi \cdot L \cdot k_{mem}} \frac{1}{h_{shellside} \cdot A_{outer}}, \tag{8}$$

where h is a function of thermal conductivity, k and the Nusselt number, Nu.

$$h_i = Nu_i \frac{k_i}{D_i}, (i = \text{tubeside, shellside}) \tag{9}$$

where Nu is an empirical function depending on the direction of the flow:

$$Nu = 0.023\, Re^{0.8}\, Pr^{0.4}, \begin{pmatrix} 0.7 \leqslant Pr \leqslant 160 \\ Re > 10000 \end{pmatrix} \quad \text{internal flow,} \tag{10}$$

$$Nu = x\, Re^{y}\, Pr^{1/3} \quad \text{external flow.} \tag{11}$$

3.3. Mass transfer

The vapor mass transfer between the shell and the tube side is driven by a concentration gradient of the humidity at the boundary of the membrane. Thus, the diffusion coefficient of the membrane and the concentration difference of the humidity determine the amount of vapor mass being transferred. Considering that the water mass flows at the boundaries of the membrane layer, the dynamics of the water concentration in the membrane was described as follows [18–20]. The diffusion caused by the water concentration gradient at the two boundaries makes up the mass flows of $W_{diff,mem,shell\ side}$ and $W_{diff,mem,tube\ side}$.

$$\frac{dm_{v,trans}}{dt} = \frac{d(C_{H_2O,mass} \cdot A \cdot t_{mem})}{dt} = W_{diff,mem,shell\ side} - W_{diff,mem,tube\ side}, \tag{12}$$

where C is the mass concentration ($kg\,m^{-3}$), M is the mole mass ($kg\,mol^{-1}$) and A is the membrane area (m^2).

The rate of the mass in the membrane can be described as follows:

$$W_{diff,mem,i} = M_v \cdot A \cdot D_w \cdot \frac{C_i - C_{middle}}{0.5 \cdot t_{mem}} \tag{13}$$

Hence, the diffusion coefficient of the membrane D_w is given as follows [18,21]:

$$D_w = D_\lambda \exp\left[2416\left(\frac{1}{303} - \frac{1}{T_{mem}}\right)\right], \tag{14}$$

where T_{mem} is the membrane temperature (K) and the coefficient D_λ is an empirical constant [18,21].

$$D_\lambda = \begin{cases} 10^{-6} & \lambda_{mem} < 2, \\ 10^{-6}[1 + 2(\lambda_{mem} - 2)] & 2 \leqslant \lambda_{mem} \leqslant 3, \\ 10^{-6}[3 - 1.67(\lambda_{mem} - 3)] & 3 < \lambda_{mem} < 4.5, \\ 1.25 \times 10^{-6} & \lambda_{mem} \geqslant 4.5. \end{cases} \tag{15}$$

The water concentration of both the shell and tube side is

$$C_i = \frac{\rho_{dry,mem}}{M_{mem}} \cdot \lambda_i, \quad C_{middle} = \frac{\rho_{dry,mem}}{M_{mem}} \cdot \lambda_{i,mem}, \tag{16}$$

where λ_{mem} is the mean water content in the membrane, which is defined as [18,19]

$$\lambda_{mem} = \frac{C_{H_2O,mass}/M_{H_2O}}{\frac{\rho_{dry,mem}}{M_{mem}} - 0.0126 \cdot C_{H_2O,mass}/M_{H_2O}}. \tag{17}$$

The boundary water content λ_i is a function of water activity a_i, which is calculated from the water vapor partial pressure [18,21]:

$$\lambda_i = \begin{cases} 0.043 + 17.81 \cdot a_i - 39.85 \cdot a_i^2 + 36 \cdot a_i^3, & 1 \geqslant a_i > 0, \\ 14 + 1.4(a_i - 1), & 3 \geqslant a_i > 1, \\ 16.8, & a_i \geqslant 3, \end{cases} \tag{18}$$

$$a_i = \frac{P_{v,i}}{P_{sat,i}}, \tag{19}$$

where i can be the shell or tube side.

4. Results and discussions

4.1. Verification of the model

For an assessment of the model developed, results of the simulation were compared with the experimental data for a humidifier, FC 200-780-10PP, provided by Perma Pure LLC. The stack exhaust gas conditions were T = 343.15 K, gas flow rate = dry air flow rate, RH = 100% and gas pressure = 1 atm, while the dry air conditions were T = 294.15 K, RH = 40% and gas pressure = 1 atm. Fig. 3 shows the results for the wet out temperature and the wet out dew point temperature in the counter flow design. The simulated results for both showed a slightly high temperature, 1 K, that might be caused by neglected fluid effects along the gas channels in the simplified model.

4.2. Static behaviors

The models developed were used to analyze the heat and mass transfer behaviors under different operating conditions.

The variables are the dry air flow rate, air inlet temperature and dry air inlet RH.

4.2.1. *Heat transfer*

Fig. 4 shows the simulated results of the heat transfer rate and the wet air outlet temperature of the humidifier at two different flow arrangements under various dry air inlet flow rates. It is noted that the arrangement with the counter flow showed more effective heat transfer than that with parallel flow because the logarithmic mean temperature in the counter flow was larger than that of the parallel flow. Moreover, when the dry air flow rate was increased, the heat transfer rate tended to follow because of the increased overall heat transfer coefficient. The heat transfer coefficient of the shell and tube side became increased because of the high flow velocity in both sides.

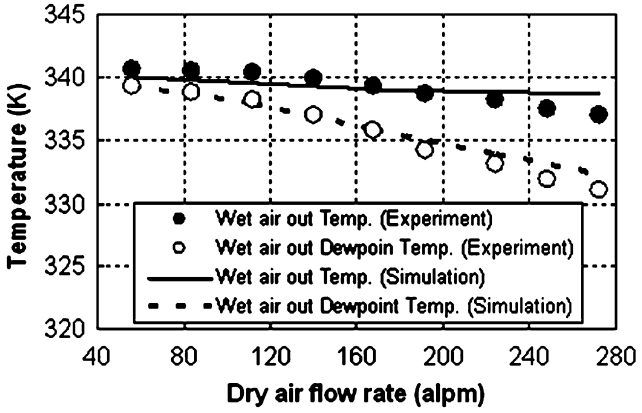

Fig. 3 – Comparison between the simulated and the measured data at various rates of dry air flow.

Fig. 5 shows the characteristics of the humidifier for a counter flow arrangement at various dry air inlet temperatures and the dry air flow rate. As the temperature of the dry air was increased, the heat transfer rate decreased because the overall heat transfer coefficient was lower because of decreased logarithmic mean temperature. Moreover, the heat transfer rate became increased when the dry air flow rate rose because the overall heat transfer coefficient was larger. When the dry air flow rate was $0.002\,kg\,s^{-1}$ that is less than that of the stack exhaust gas, the temperature of the wet air outlet rose until it matched that of the exhaust gas and remained there regardless of the temperature value of the dry air inlet gas. However, when the dry air flow rate was $0.004\,kg\,s^{-1}$ and higher than that of the fuel cell stack exhaust gas, the gradient of the wet air outlet temperature became larger even though the rate of heat transfer was decreased.

Fig. 6 shows the heat transfer characteristics of the humidifier for a counter flow arrangement at different inlet relative humidities and the dry air flow rates. As a matter of fact, the heat transfer rate was predominantly influenced by the flow rate and the temperature of the dry air and not significantly affected by the relative humidity, even though the vapor concentration in the tube side tended to follow variations in the relative humidity.

Conversely, the flow rate of the inlet air directly influenced the rate of the heat transfer. In fact, the heat transfer coefficient in the tube side became larger when the flow rate of the inlet air was increased. In addition, the temperature of the wet air outlet decreased simply because of the relatively high air mass, where the temperature was not affected by the increased rate of heat production.

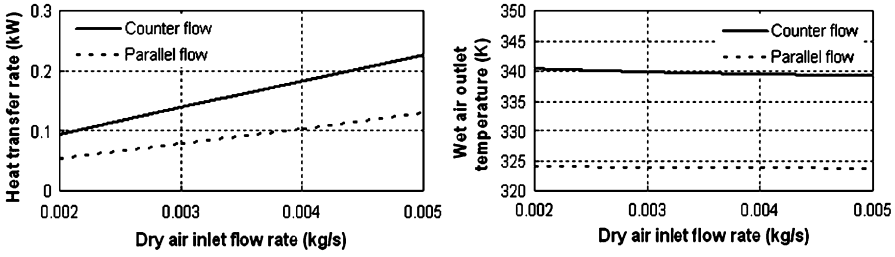

Fig. 4 – Comparison of two different flow arrangements at different dry air flow rates (fuel cell exhaust air condition: T = 343.15 K, exhaust air flow rate = dry air flow rate, RH = 100% and pressure = 1.3 atm. Dry air condition: T = 298.15 K, RH = 30% and pressure = 1.3 atm).

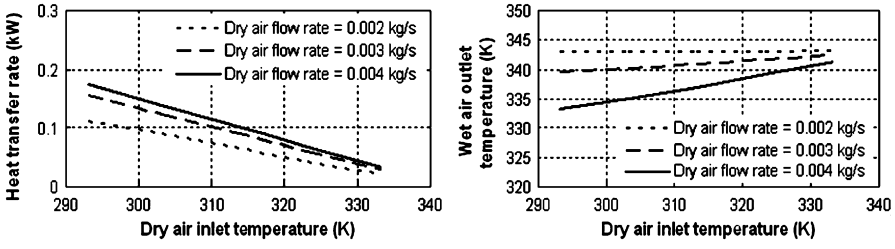

Fig. 5 – Comparison of two flow arrangements at different dry air inlet temperatures (fuel cell exhaust air condition: T = 343.15 K, flow rate = $0.003\,kg\,s^{-1}$, RH = 100% and pressure = 1.3 atm. Dry air condition: RH = 30% and pressure = 1.3 atm).

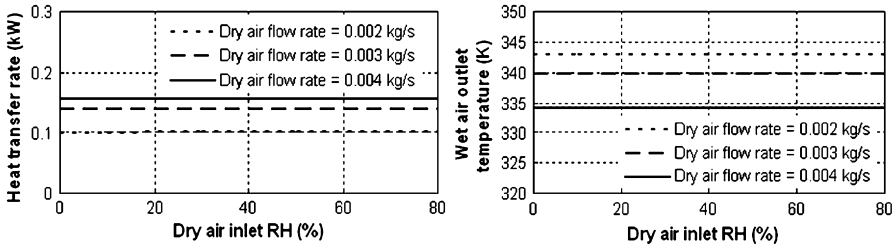

Fig. 6 – Comparison of two flow arrangements at different air inlet RH (fuel cell exhaust air condition: $T = 343.15\,K$, flow rate $= 0.003\,kg\,s^{-1}$, RH = 100% and pressure = 1.3 atm. Dry air condition: $T = 298.15\,K$ and pressure = 1.3 atm).

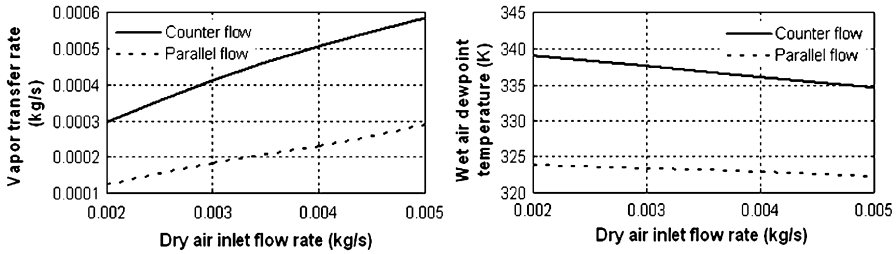

Fig. 7 – Comparison of two different flow arrangements at various dry air flow rates (fuel cell exhaust air condition: $T = 343.15\,K$, exhaust air flow rate = dry air flow rate, RH = 100% and pressure = 1.3 atm. Dry air condition: $T = 298.15\,K$, RH = 30% and pressure = 1.3 atm).

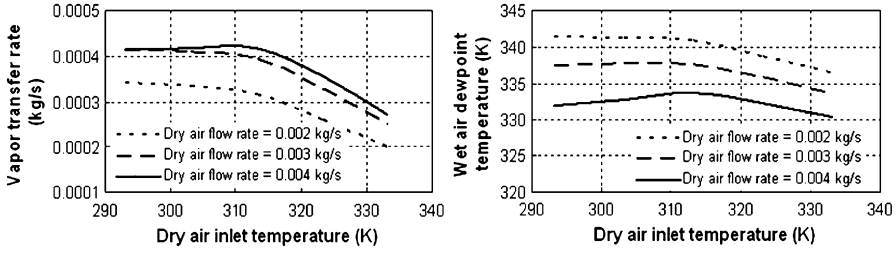

Fig. 8 – Comparison of two flow arrangements at different dry air inlet temperatures (fuel cell exhaust air condition: $T = 343.15\,K$, flow rate $= 0.003\,kg\,s^{-1}$, RH = 100% and pressure = 1.3 atm. Dry air condition: RH = 30% and pressure = 1.3 atm).

4.2.2. *Vapor transfer*

Fig. 7 shows simulated results of the vapor transfer rate and the wet air dew point temperature of the humidifier at two different flow arrangements under various dry air inlet flow rates. The diffusion coefficient is a function of the temperature and water content in the membrane, where the coefficient in the counter flow became larger than that in the parallel flow at elevated membrane temperatures. In addition, when the dry air flow rate was increased, the vapor transfer rate became higher because of the decreased vapor concentration caused by the low vapor pressure in the tube side. On the other hand, the wet air dew point temperature rose at the low rate of the inlet flow because of the high vapor pressure on the tube side, even at the low vapor transfer rate.

Fig. 8 shows the characteristics of the humidifier for the counter flow arrangement at various dry air inlet temperatures and dry air flow rates. The results showed the highest vapor transfer at about 310–315 K dry air temperature. Above the dry air temperature of 310–315 K, the water activity became lower because the relatively high temperature on the shell side decreased the water concentration. Consequently, the vapor transfer rate decreased. Below the dry air temperature of 310–315 K, the mass transfer was limited by the saturation on the tube side. In addition, when the flow rate of the dry air was increased, the rate of the vapor transfer was increased and the temperature of the wet air dew point became lower.

Fig. 9 shows the characteristics of the humidifier for a counter flow arrangement at different inlet relative humidities and dry air flow rates. When the dry air inlet RH was increased, the water concentration on the tube side tended to increase and consequently the vapor transfer rate decreased. In addition, when the flow rate of the dry air ($0.004\,kg\,s^{-1}$) was higher than that of the exhaust gas flow from the stack, the vapor transfer rate was the same as the dry air flow rate of $0.003\,kg\,s^{-1}$. In fact, the vapor saturation pressure decreased because of the lower temperature of the wet air outlet caused by an increased dry air flow rate. As a result, the mass transfer was limited by the saturation conditions on the tube side.

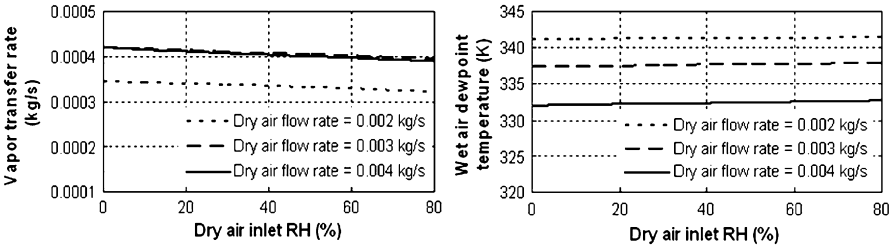

Fig. 9 – Comparison of two flow arrangements at different air inlet RH (fuel cell exhaust air condition: $T = 343.15\,K$, flow rate $= 0.003\,kg\,s^{-1}$, RH = 100% and pressure = 1.3 atm. Dry air condition: $T = 298.15\,K$ and pressure = 1.3 atm).

4.3. *Effect of geometric parameters*

Geometric design parameters considered in this study were the thickness of the membrane, diameter and the length of a tube, the number of tubes and the housing diameter. In addition, it was assumed that the strength of materials and pressure drops inside the materials were negligible and that the flow rate of the inlet gas was identical with that of the exhaust gas. First, the dependence of the design parameters aforementioned on changes of the flow rate was investigated, where the counter flow arrangement was used because of its better performance in heat and mass transfer. The operating conditions of the shell-and-tube type gas-to-gas membrane humidifier are listed in Table 2.

Fig. 10 shows the effects of membrane thickness on the heat and vapor transfer rates in a counter flow arrangement. As the membrane becomes thicker, the vapor transfer rate is reduced, while the heat transfer rate was not affected by the thickness of the membrane. At a membrane thickness of 0.0001 m, the increased rate of vapor transfer was decreased, particularly at the high flow rates, simply because the influence of the membrane thickness on mass transfer is higher than that of the water concentration.

Fig. 11 shows the effects of the membrane tube inner diameter on the heat and vapor transfer rates in a counter flow arrangement. A large inner diameter of the tube increased the heat transfer rate because the flow velocity on the shell side was faster and the heat transfer coefficient of shell side was higher. Moreover, the vapor transfer rate increased because of the increased surface area of the membrane.

Fig. 12 shows the effects of the active membrane tube length on the heat and vapor transfer rates in a counter flow arrangement. The length of the active membrane tube did not significantly affect the heat transfer rate, while the vapor transfer rate increased because of the increased surface area of the membrane.

Effects of the tube number on the heat and vapor transfer rates in a counter flow arrangement are shown Fig. 13. Large numbers of membrane tubes decreased the heat transfer coefficient of tube side, while that on the shell side increased. As a result, the overall heat transfer coefficient increased and the heat transfer rate decreased, while the vapor transfer rate was higher because of the increased surface active area of the membrane.

The effects of the inner diameter of the humidifier housing on the heat and vapor transfer rates in a counter flow arrangement are shown in Fig. 14. A large diameter of the shell decreased the heat transfer coefficient in the shell side because of the low flow velocity in the shell side. As a result, the heat transfer rate decreased because of the reduced overall heat transfer coefficient. In addition, the mass transfer rate of vapor decreased because of the decreased diffusion coefficient of the membrane caused by the low heat transfer coefficient and the temperature drop in the membrane.

Table 2 – Operating conditions

Parameters	Value
Exhaust air	
Inlet temperature	343.15 K
Inlet gas flow rate	0.002–0.005 $kg\,s^{-1}$
Relative humidity	100%
Inlet pressure	1.3 bar
Dry air	
Inlet temperature	298.15 K
Inlet gas flow rate	0.002–0.005 $kg\,s^{-1}$
Relative humidity	30%
Inlet pressure	1.3 bar

4.4. *Dynamic behaviors*

When the stack is operated with a humidifier, the operation conditions continuously vary as loads change. The amount of down-streaming air supplied from an air blower is determined by the amplitude of the load current and subsequently the dry air flow rate for the humidifier also varies. On the other hand, humidification of the dry air is affected by the flow rate of the exhaust gas from the stack. Thus, it is important to investigate the dynamic relationship between the dry air and the stack exhaust air, where a multi-step flow rate was applied by assuming that other operating conditions were constant.

Fig. 15 shows dynamic responses of the humidifier at a step change of the dry air inlet flow rate (a), where the exhaust gas conditions assumed that $T = 343.15\,K$, gas flow rate $= 0.003\,kg\,s^{-1}$, RH = 100% and gas pressure = 1.3 atm, while the dry air conditions were $T = 298.15\,K$, RH = 30% and gas pressure = 1.3 atm. Figs. 15 (b)–(e) are the resulting heat and vapor transfer rates, temperature and relative humidity of the wet air outlet, respectively.

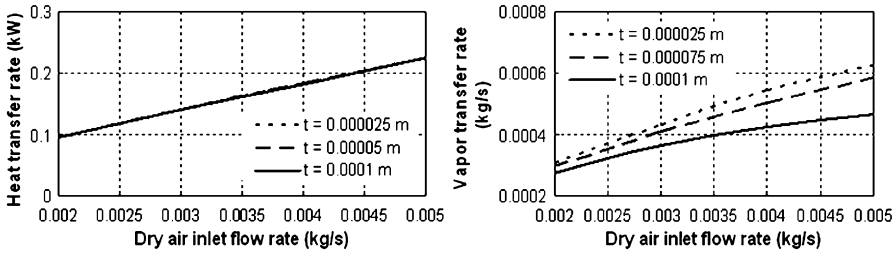

Fig. 10 – Effects of membrane tube thickness on performance at different dry air flow rates (*t*: thickness of the membrane tube).

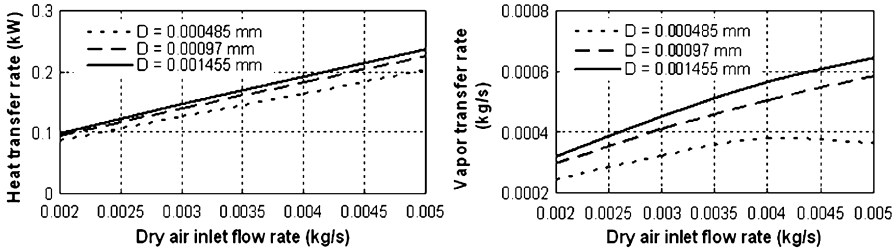

Fig. 11 – Effects of membrane tube inner diameter on performance at different dry air flow rates (*D*: inner diameter of the membrane tube).

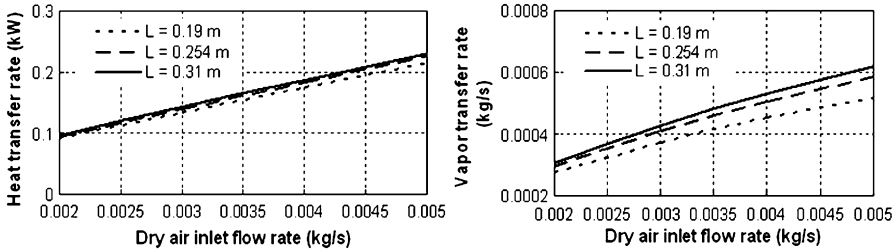

Fig. 12 – Effects of active membrane tube length on the performance at different dry air flow rates (*L*: active length of the membrane tube).

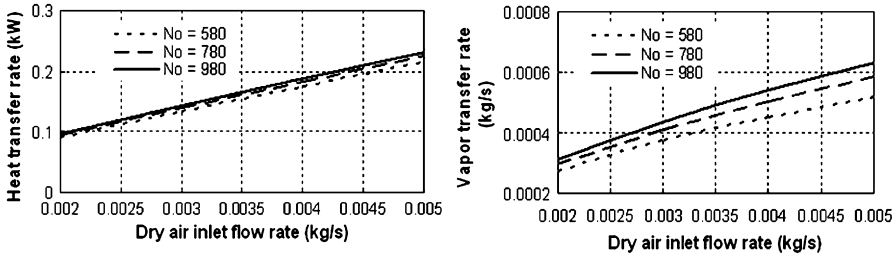

Fig. 13 – Effects of membrane tube number at various dry air flow rates (No: number of the membrane tubes).

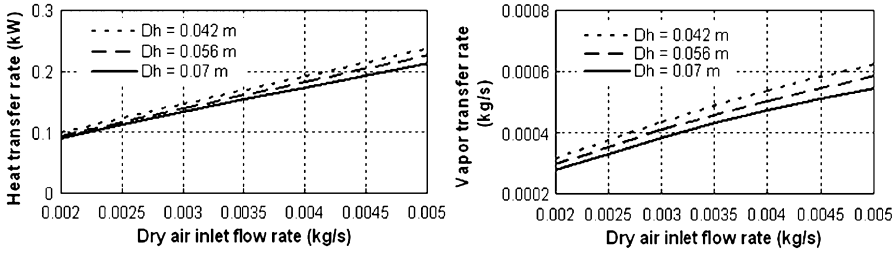

Fig. 14 – Effect of inner diameter of humidifier housing on the performance at different dry air flow rates (Dh: inner diameter of the humidifier housing).

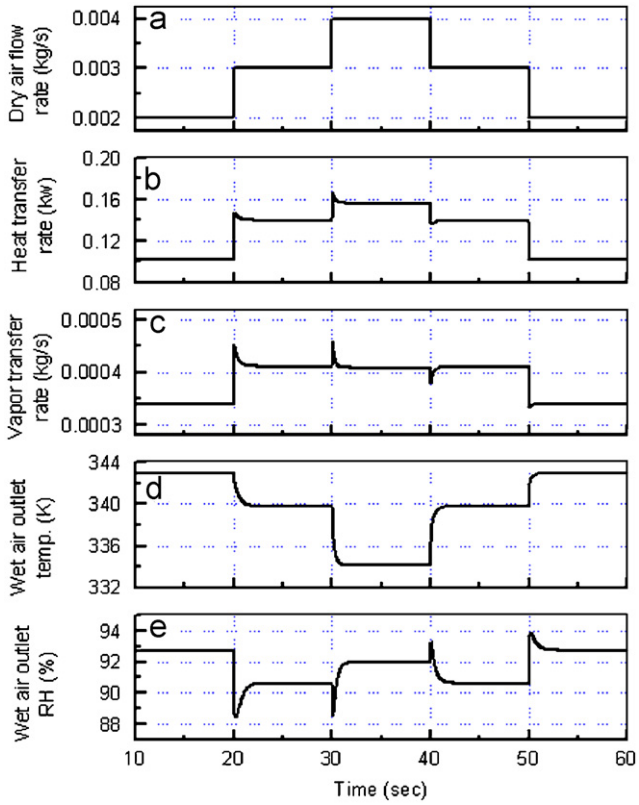

Fig. 15 – Step responses of the humidifier on dry air flow rates.

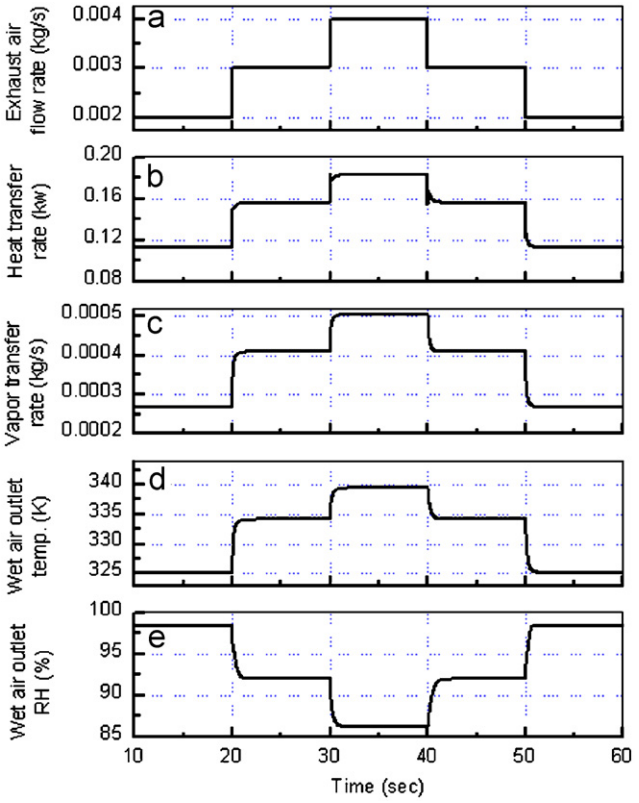

Fig. 16 – Step responses of the humidifier on stack exhaust air flow rates.

The heat transfer rate corresponded with the dry air flow rate. In general, the dry air flow rate directly affects the vapor transfer rate because an increased flow rate reduces the vapor pressure. As a result, water concentration on the tube side became lower and subsequently the vapor transfer rate increased. However, when the flow rate of the dry air ($0.004\,kg\,s^{-1}$) was higher than that of the exhaust gas, the vapor transfer rate remained the same because of the mass transfer limited by the high saturation of the inlet gas on the tube side.

At a sudden increase of the dry air flow rate, the vapor transfer rate showed an overshoot behavior, which was caused by different diffusion behaviors of the vapor transfer in the membrane. When the dry air flow rate was abruptly increased, the vapor mass remained the same as before at that instant, while the vapor pressure was decreased and subsequently the vapor concentration became lower. Thus, the vapor transfer rate rapidly increased and finally reached a steady state. When the flow rate of the dry air was increased, the temperature of the wet air outlet dropped.

Fig. 16 shows dynamic responses of the humidifier at a step change of the stack exhaust air inlet flow rate (a), which includes the heat transfer rate (b), the vapor transfer rate (c), the temperature (d) and the relative humidity (e) of the wet air outlet. It was assumed that the exhaust air was with T = 343.15 K, RH = 100% and gas pressure = 1.3 atm, while the dry inlet air was with T = 298.15 K, gas flow rate = $0.004\,kg\,s^{-1}$, RH = 30% and gas pressure = 1.3 atm. According to this analysis, the heat and vapor transfer rate tended to follow the flow rate of the stack exhaust air because of the fully saturated relative humidity and constant temperature assumed as a condition for the exhaust air. Both of these showed a highly damped behavior. The temperature of the wet air outlet followed the increase of the flow rate of the stack exhaust air, while the relative humidity was reduced.

The analysis above revealed a possible control strategy that allows the inlet air to be manipulated by adding an extra vent valve that serves to regulate the flow rate of the exhaust air. It might be particularly effective at high currents where the flooded water on the cathode can be properly removed.

5. Conclusions

The gas-to-gas membrane is preferred in mobile applications because of its compactness and high efficiency. We developed a transient model for the shell-and-tube type gas-to-gas membrane humidifier and compared the results with experimental data provided by a manufacturer. The model is based on the principle of thermodynamics; the heat and mass transfer in the two control volumes. The model was used to analyze sensitivities of the geometric parameters on the performance under different operating conditions and transient behaviors. The findings are summarized as follows:

- The heat and mass transfer in the counter flow arrangement were more effective than those in the parallel flow arrangement.

- The increased flow rate of the dry gas increased the transfer rate of the heat and vapor mass. In particular, the wet air dew point temperature rose at low rates of inlet flow.
- The vapor transfer rate reached the highest value at dry air inlet temperatures of 310–315 K, while the relative humidity of the inlet gas did not significantly affect the heat transfer rates.
- The heat transfer rate was not significantly affected by geometric parameters of the humidifier. However, the rate of the vapor mass transfer increased, as the inner diameter, length and the number of the tubes increased.
- Possibly, the flow rate of the stack exhaust air can be effectively used to control water balance at high currents.

Acknowledgments

The authors gratefully acknowledge the technical discussions and experimental data provided by Mr. Matthew Powers of Perma Pure LLC, USA.

REFERENCES

[1] Zawodzinski Jr TA, Derouin C, Radzinski S, Sherman RJ, Smith VT, Springer TE, et al. Water uptake by and transport through Nafion® 117 membranes. J Electrochem Soc 1993;140(4):1041–7.
[2] Ren X, Gottesfeld S. Electro-osmotic drag of water in poly (perfluorosulfonic acid) membranes. J Electrochem Soc 2001;148(1):87–93.
[3] Larminie J, Dicks A. Fuel cell systems explained. 2nd ed. New York: Wiley; 2003.
[4] Ceraolo M, Miulli C, Pozio A. Modeling static and dynamic behavior of proton exchange membrane fuel cells on the basis of electro-chemical description. J Power Sources 2003;113:131–44.
[5] Cooper JS. Design analysis of PEMFC bipolar plates considering stack manufacturing and environment impact. J Power Sources 2004;129:152–69.
[6] Williams MV, Begg E, Bonville L, Russell Kunz H, Fenton JM. Characterization of gas diffusion layer for PEMFC. J Electrochem Soc 2004;151(8):1173–80.
[7] Yan Q, Toghiani H, Wu J. Investigation of water transport through membrane in a PEM fuel cell by water balance experiments. J Power Sources 2006;158:316–25.
[8] Zhou B, Huang W, Zong Y, Sobiesiak A. Water and pressure effects on a single PEM fuel cell. J Power Sources 2006;155:190–202.
[9] Wood III DL, Yi JS, Nguyen TV. Effect of direct liquid water injection and interdigitated flow field on the performance of proton exchange membrane fuel cells. Electrochim Acta 1998;43(24):3795–809.
[10] Ito T, Yuan, J Sunden B. Water recover schemes and effect on the water/thermal balances for a 100 kw PEMFC system. In: The 4th international conference on fuel cell science, engineering and technology, FUELCELL 2006-97114, 2006.
[11] Carlson EJ, Kopf P, Sinha J, Sriramulu S, Yang Y. Cost analysis of PEM fuel cell systems for transportation. Subcontract Report (NERL/SR-560-39104); December 2005.
[12] Zhang LZ, Jiang Y, Zhang YP. Membrane-based humidity pump: performance and limitations. J Membr Sci 2000;171:207–16.
[13] Daud WRW. Shortcut design method for reverse osmosis tubular module: the effect of varying trans-membrane pressure and concentration polarization. Desalination 2006;201:297–305.
[14] Chen D, Peng H. A thermodynamic model of membrane humidifiers for PEM fuel cell humidification control. J Dyn Syst Meas Control 2005;127:424–32.
[15] Perma Pure LLC. 〈http://www.permapure.com/〉.
[16] Sonntag RE, Borgnakke C, Van Wylen GJ. Fundamentals of thermodynamics. 5th ed. New York: Wiley; 1998.
[17] Incropera FP, Dewitt DP. Fundamentals of heat and mass transfer, 4th ed., 1996.
[18] Springer TE, Zawodzinski TA, Gottesfeld S. Polymer electrolyte fuel cell model. J Electrochem Soc 1991;138(8):2334–41.
[19] Shan Y, Choe SY. A high dynamic PEM fuel cell model with temperature effect. J Power Sources 2005;145:30–9.
[20] Nguyen TV, White RE. A water and heat management model for proton-exchange-membrane fuel cells. J Electrochem Soc 1993;140(8):2178–86.
[21] Pukrushpan JT, Peng H, Stefanopoulou AG. Simulation and analysis of transient fuel cell system performance based on a dynamic reactant flow model. In: Proceeding of 2002 ASME international mechanical engineering congress & exposition. IMECE2002-DSC-32051 2002.